Using the Amplitude Variation of a Reverberation Chamber Channel to Predict the Synchronization of a Wireless Digital Communication Test System

Ray R. Tanuhardja[1,2], Luis A. Gonzalez[1], Chih-Ming Wang[1], William F. Young[1], Kate A. Remley[1], and John M. Ladbury[1]

[1]Communications Technology Laboratory
National Institute of Standards and Technology
Boulder, CO, USA, 80305
william.young@nist.gov and kate.remley@nist.gov

[2]Electrical Engineering Department
University of Twente
Enschede, The Netherlands

***Abstract*—We discuss the use of a metric based on the amplitude variation of a channel in the signal bandwidth to predict whether or not a digital wireless communication test system receiver will be able to demodulate a test signal. This metric is compared to another method consisting of the correlation calculated across the channel. A logistic regression analysis is used to provide a normalized assessment of the effectiveness of each metric as a predictive tool. We show that both metrics provide similar predictive capabilities, with the peak-to-minimum being significantly easier to calculate.**

Keywords—coherence bandwidth; correlation bandwidth; over-the-air measurement; reverberation chamber; wireless channel; wireless communication test system.

I. INTRODUCTION

Reverberation chambers have been used in the past for electromagnetic compatibility (EMC) tests [1, 2]. Research is now moving towards use of reverberation chambers for testing wireless devices, such as cellular phones, WiFi devices, and RFID tags [3, 4, 5]. Researchers have also investigated the effect of the reverberation chamber environment on orthogonal frequency-division multiplexing signals [6, 7] and the bit error rate of signals demodulated by test systems [8, 9]. A reverberation chamber can generate various Rician multipath propagation environments [10, 11] and many widely varying channels in a short amount of time by simply changing the boundary conditions within the chamber. Reverberation chambers provide a repeatable test environment that can simulate the large range of radio environments in which wireless devices typically operate, making these chambers of great interest to manufacturers of wireless devices as a testing environment.

Digitally-modulated signals transmitted by wireless communication devices are more complex than the continuous waves used in EMC tests. When continuous waves are transmitted, we typically do not need to take into account the instantaneous frequency response of the channel generated in a reverberation chamber because the signals are narrowband. However, digitally modulated signals can easily use up to tens of megahertz of bandwidth and the multipath environment in a reverberation chamber (unloaded) does not typically provide a frequency-flat fading channel [1, 11]. For this reason, a thorough understanding is needed of how the channels in a reverberation chamber affect wideband signals and, ultimately, how that information can be used to predict which digitally-modulated signals will pass through the reverberation-chamber channel with sufficiently low distortion that the receiver can demodulate them.

Prior work has investigated the reverberation-chamber induced bit error rate (BER) of binary phase-shift-keying (BPSK) modulated signals with a bandwidth of less than ~1 MHz [8, 9]. This and other work (*e.g.*, [11, 12]) demonstrated that loading the reverberation chamber with absorbers decreases the chamber-induced BER. The amount of loading was determined such that the average coherence bandwidth (the bandwidth over which frequencies are appreciably correlated) exceeded the signal bandwidth. The coherence bandwidth was found by averaging over all mode-stepped samples. Essentially, the averge coherence bandwidth was used as a metric to predict chamber-induced distortion.

This paper will focus on predictive metrics related to the instantaneous channel (the channel created for each mode-stepped sample) because wireless devices and receivers must operate in the instantaneous channel. We consider the behavior of a 1 MHz wide QPSK signal with a 2.4 GHz center frequency. Instead of looking at the BER, we will look at whether or not the receiver is able to synchronize to the test signal and assess system performance with the RMS-normalized error vector magnitude (EVM_{RMS}). As in [8], we study the impact of the reverberation chamber on the performance of the wireless digital communication receiver at the fundamental level by not implementing additional protocols that assist in error correction, handshaking and synchronization.

The model of [13] indicates that the amplitude variation of a multipath fading channel, here termed the *a*-factor, can play a significant role in determining whether or not two signals at different frequencies within the channel bandwidth are

appreciably correlated. This metric is relatively easy to compute by finding the channel's peak and minimum in the signal bandwidth. We compare the effectiveness of the *a*-factor in predicting test system performance in a reverberation chamber to a metric based on the correlation calculated over the channel bandwidth (essentially the coherence bandwidth calculated over only the channel). We investigate correlation metrics based on both the complex channel data and the envelope only. All three of these metrics are computed from the instantaneous channel created at each stirred state in the reverberation chamber. We use a binomial logistic regression analysis to compare how well the different metrics are able to predict whether or not the digital wireless communication test system synchronizes through the channel.

II. Coherence Bandwidth and the *a*-factor

Complex physical models of the mobile transmission path are often utilized to take into account the multipath environment that most wireless communication systems experience. A mathematical model was developed in [13] to quantify the statistics and correlation properties of the envelopes and the phases of narrowband signals at two different frequencies that propagate through a multipath environment. This model is potentially useful for studying reverberation chambers, since a reverberation chamber creates a high multipath environment.

Consider the situation in Fig. 1. The transmit antenna emits two signals at different frequencies into a channel. In a multipath environment, the fields at the receive antenna are assumed to be the sum of a large number of plane waves of random amplitudes, phases, and arrival angles. The two signals experience the channel differently since the frequency difference causes a difference in path length and, thus, a difference in propagation time delays. The two signals can be considered statistically independent if the frequency separation between them is large enough and the difference in time delays is significant. The coherence bandwidth in [13] is defined as the maximum frequency separation between two signals, such that the two signals are still statistically strongly correlated.

From the assumption that the phases of the individual waves that form the received signals are uniformly distributed and are independent random variables, it follows that the fields are wide-sense stationary with respect to the ensemble average. If the number of waves is large, then the difference between the time and ensemble averages becomes small. Therefore, the statistical properties can be calculated based on only the ensemble averages as long as the number of waves, that is, multipath components, is large.

We can then determine the joint density function of these two received fields. The correlation of the envelopes of the signals may be found by use of the joint density function as given in [13]

$$\rho_e(s,\tau) \doteq \lambda^2 = \frac{J_0^2(\omega_m \tau)}{1+s^2\sigma^2} \ , \tag{1}$$

where J_0 represents the zeroth order Bessel function of the first kind, ω_m the Doppler shift in radians, τ the time delay in seconds, s the separation frequency in radians, and σ the RMS

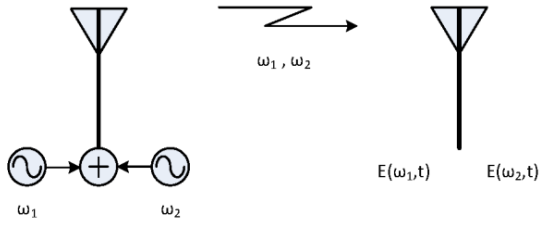

Fig. 1. Basic two-carrier setup to determine the coherence bandwidth of a channel (after [13]).

time-delay-spread in seconds. These delays are relative to the first detectable signal arriving at the receiver. If the correlation is equated to 0.5 and the time delay τ is assumed to be 0, then the coherence bandwidth can be related to the RMS delay spread as

$$B_c = \frac{1}{2\pi\sigma} \ \text{[Hz]} \ , \tag{2}$$

where B_c represents the single-sided coherence bandwidth.

The autocorrelation threshold of 0.5 was chosen in [13] by determining the probability that the signal envelope at frequency ω_2 exceeds a times the envelope at frequency ω_1. This probability may be given as

$$P[r_2 \geq a r_1] \triangleq P(a,\lambda) = \frac{1}{2} + \frac{1}{2}\frac{(1-a^2)}{\sqrt{(1+a^2)^2 - 4\lambda^2 a^2}} \ , \tag{3}$$

with r_1 and r_2 the envelope amplitudes at frequencies ω_1 and ω_2, and a the factor with which r_2 exceeds r_1 [13]. The probability described by (3) indicates what difference in magnitude between frequency components the receiver can expect to see in the multipath environment under investigation. The receiver implementation will determine whether or not the received signal is processed correctly for a given *a*-factor and accompanying probability. The probability $P(a,\lambda)$ described by (3) is plotted against $s\sigma$ in Fig. 2 for several values of a.

Fig. 2 describes whether or not the variation in amplitude due to multipath fading at the two frequencies is appreciably correlated. The coherence bandwidth is the frequency separation beyond which the channel is considered to be uncorrelated. In Fig. 2, the coherence bandwidth (in radians) is equal to the separation s when $s\sigma = 1$. For two signals with a given separation s, the coherence bandwidth will be narrower than the signal bandwidth to the right of $s\sigma = 1$ on the x axis. For channels corresponding to this case, the probability of the

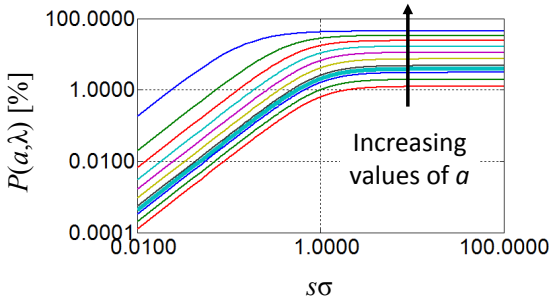

Fig. 2. The probability from (3) that r_2 is a times larger than r_1 plotted for different a values (after [13]).

two signals having appreciably different amplitudes is relatively high (as shown on the *y* axis) for all *a*-factor values. Thus, the receiver may have difficulty synchronizing. For channels to the left of $s\sigma = 1$ on the *x* axis, the value of the *a*-factor will play a significant role in determining the probability of significant amplitude variation within the channel, even for a wide coherence bandwidth.

In practice, receivers will experience a distribution of *a*-factor values. This distribution can be estimated in a reverberation chamber measurement from the peak-to-minimum value for every channel. If we know what peak-to-minimum values the receiver can process, then an estimate can be made of how many channels in a given reverberation-chamber set-up is the receiver able to function adequately; i.e., the receiver can determine what constellation symbol was sent.

III. Experimental Work

To investigate the use of the amplitude variation as a metric for predicting receiver performance, we conducted measurements of modulated signals in reverberation chambers with a wireless test system. We computed the EVM_{RMS} for each mode-stepped sample (or channel). Leaving the set-up within the chamber undisturbed, we then found the corresponding *a*-factor and correlation bandwidth from measurements made with a vector network analyzer.

A. Measurement set-up

An overview of the measurement set-up is shown in Fig. 3. All experiments in this paper were performed with a vector signal transceiver (VST) and a vector network analyzer (VNA) in two reverberation chambers at the National Institute of Standards and Technology (NIST). The dimensions of these two chambers are 150 cm x 146 cm x 118 cm (small chamber), and 4.6 m x 3.1 m x 2.8 m (large chamber). Two different chambers were used to investigate reproducibility. Antennas were strategically placed to minimize antenna proximity to both metallic and RF absorbing materials [1, 14] and to minimize the line-of-sight component between the antennas. Measurements were made at four different antenna locations for each loaded-chamber absorber configuration.

In the small chamber, RF absorbers of size 30 cm x 30 cm x 15 cm were placed on Styrofoam™ blocks spaced at a distance between absorbers and metallic walls of more than half a wavelength. In the large chamber, absorbers of size 60 cm x 60 cm x 15 cm were placed in stacks of three and these stacks were also placed more than half a wavelength in distance between the other stack and metallic surfaces. The absorbing surface area was scaled from the small chamber to the large chamber at a ratio 1:5. The transmit antenna in all measurements was a wideband horn antenna. The receive antenna was a horn, a helix, or a patch antenna. For both the VST and VNA measurements, we acquired data at 360 paddle positions, where the single rotating paddle moved in 1° increments.

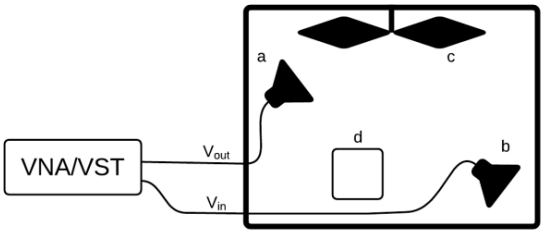

Fig. 3. Schematic overview of the reverberation chamber and measurement setups, where *a* is the transmitting antenna, *b* the receiving antenna, *c* the paddle and *d* the absorber. The VNA measured the incident and reflected traveling waves at the reverberation chamber reference place. The VST was connected to the same reference plane used in the VNA measurements.

The transmitter of the VST was used to generate a QPSK signal with a center frequency of 2.412 GHz, a bandwidth of 1 MHz and a root-raised cosine filter of length 16 and alpha of 0.35. The VST transmitted 41 packets of 564 symbols at each stationary paddle position. For all 360 paddle positions, we acquired the EVM_{RMS} and the signal-to-noise ratio (SNR). The SNR was kept sufficiently high to ensure that Gaussian noise was not a contributing factor to the degradation of the signal; most of the errors in transmission can therefore be attributed to the distortion in the channel.

EVM describes the difference between a measured symbol and its ideal constellation point. Because of its normalized nature EVM_{RMS} is well suited to characterize modulation schemes of varying order and complexity; this has motivated its use in several communications standards. Our study made use of the EVM_{RMS}, defined as follows [15]:

$$EVM_{\mathrm{RMS}} = \sqrt{\frac{\frac{1}{N}\sum_{k=1}^{N}\left|S_{\mathrm{error,k}}\right|^2}{\frac{1}{N}\sum_{k=1}^{N}\left|S_{\mathrm{ideal,k}}\right|^2}} \quad , \tag{4}$$

where N is the total number of symbols measured, $S_{\mathrm{ideal,k}}$ is the k^{th} normalized symbol, $S_{\mathrm{meas,k}}$ is the normalized symbol of the k^{th} symbol measured, and $S_{\mathrm{error,k}}$ is the normalized error vector (i.e., $S_{\mathrm{meas,k}}$ $S_{\mathrm{ideal,k}}$). The normalization corresponds to the RMS value taken over all of the symbols.

The test system finds synchronization by searching for a predefined bit stream in the received signal at the receive antenna in the reverberation chamber. If that bit stream is corrupted by the channel, the receiver may not successfully synchronize, resulting in a high value of EVM_{RMS}.

We used the EVM_{RMS} to make a distinction between paddle positions where the receiver was able to properly demodulate the signal (sync case) and paddle positions where the receiver was unable to demodulate the signal (non-sync case). We defined the sync case if the variance of the EVM_{RMS} was less than 10 percent. Fig. 4 shows the distinct difference in EVM_{RMS} measurements between a sync case and a non-sync case.

To characterize the corresponding channel, S-parameters were collected with a VNA for the same 360 paddle positions. Data were collected from 2.387 GHz to 2.437 GHz with a frequency step of 1 kHz. A VNA dwell time of 20 µs was used. We determined the coherence bandwidth, the received

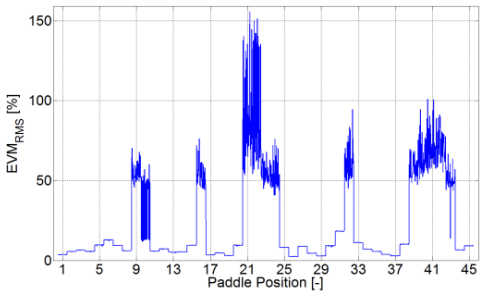

Fig. 4. The EVM_{RMS} for different paddle positions. The value of EVM_{RMS} at paddle positions where the digital wireless communication test system synchronizes is lower than the values of EVM_{RMS} at paddle positions where the test system does not synchronize. In this measurement setup, the large reverberation chamber was loaded with two stacks of three absorbers. A dual-ridge guide horn was used as the transmit antenna and a patch as the receive antenna.

correlation bandwidth (defined below) and the peak-to-minimum ratio from the transmission parameter S_{21}.

To find the coherence bandwidth, for each paddle position, the autocorrelation function was calculated over a predefined bandwidth using the following function [9, 11, 12]:

$$R_n(\Delta f) = \int_{f_{start}}^{f_{stop}} S_{21_n}(f) S_{21_n}^*(f+\Delta f)\mathrm{d}f \ , \qquad (5)$$

where S_{21n} is the complex transfer function of the instantaneous channel at paddle position n, * denotes the complex conjugate, Δf is the bandwidth over which the autocorrelation function is determined, and f_{stop} f_{start} denotes the evaluation bandwidth.

The electromagnetic field does not necessarily have the same statistics over all of the paddle positions, as pointed out in [16] and the wireless communication test system receiver does not experience the signals outside its signal bandwidth. Therefore, we evaluated the correlation over the signal bandwidth and for each paddle position at a fixed threshold. We define the correlation over this bandwidth as the "received correlation bandwidth" (B_r), which will have a maximum value that is the same as our signal bandwidth, 1 MHz. If the chosen threshold is too low, then the B_r will have the maximum value at all paddle positions. However, if the chosen threshold is too high, then the range of B_r of the synchronized and unsynchronized cases will overlap. A threshold of 0.5 ensures that the overlap is small. Furthermore, this threshold value is consistent with the value chosen in [13]. We assessed the correlation using both the complex S_{21} data, which we denote B_{rc}, and using the envelope of the S_{21} data given by B_{re}.

The *a*-factor was obtained by determining the peak-to-minimum of the magnitude of the S_{21} data within the signal bandwidth. Although we used a VNA to obtain the S_{21} data, a spectrum analyzer would also provide the peak-to-minimum value.

B. Experimental Results

Table I shows measured results for several chamber configurations, including the percentage of cases for which the VST receiver was able to synchronize and demodulate the signal, as well as the coherence bandwidth. The coherence bandwidth was calculated over a much wider bandwidth (50 MHz) than the signal bandwidth and was averaged over all paddle angles in accordance with [9, 11, 12]. The coherence bandwidth B_c was determined for several different threshold values, where the higher thresholds define a narrower coherence bandwidth for a given channel.

TABLE I. SYNCHRONIZED CASES AND THE COHERENCE BANDWIDTH FOR DIFFERENT MEASUREMENT SET-UP CONFIGURATIONS

Measurement setup		Synchronized cases [%]	Coherence ($2\times B_c$) Bandwidth [MHz]		
			0.5	*0.7*	*0.9*
Small Reverberation Chamber	0 Abs Helix	39.2	1.9	1.0	0.48
	0 Abs Horn	47.8	2.0	1.1	0.50
	0 Abs Patch	37.5	1.8	1.0	0.48
	1 Abs Helix	85.6	7.9	4.2	1.8
	1 Abs Horn	83.3	8.5	4.3	1.8
	1 Abs Patch	85.0	6.9	3.9	1.8
	2 Abs Helix	92.2	14	7.3	1.4
	2 Abs Horn	91.7	14	7.2	3.0
	2 Abs Patch	92.2	14	7.4	3.0
Large Reverberation Chamber	0 Abs Helix	12.5	0.68	0.39	0.19
	0 Abs Horn	10.3	0.71	0.41	0.19
	0 Abs Patch	8.1	0.69	0.69	0.69
	3 Abs Helix	50.0	2.4	1.4	0.65
	3 Abs Horn	53.1	2.3	1.4	0.64
	3 Abs Patch	43.9	2.8	1.5	0.68
	6 Abs Helix	66.4	4.2	2.3	1.1
	6 Abs Horn	61.4	4.8	2.7	1.2
	6 Abs Patch	64.7	3.9	2.3	1.0

We see, as expected, that the receiver is not able to synchronize for unloaded and lightly loaded cases, and that B_c increases with loading. Note that if error correction was used, the successful synchronization rate would be much higher.

Fig. 5 shows several values of the magnitude of S_{21} over the channel bandwidth. The lower six (red) curves denote channels in which the VST could not synchronize and the upper curves (blue) denote those in which it could synchronize. In cases where synchronization was not obtained, the channels either had frequency-selective fades or the magnitude of the spectrum had a slope of more than 5 dB across the channel. When the channel distortion exceeds a certain level, the system cannot successfully determine what the transmitted constellation points are. B_{rc}, B_{re}, and the a-factor may be used to determine the conditions for synchronization (see Section IV).

Histograms and a Gaussian kernel fit are plotted for B_{rc} and

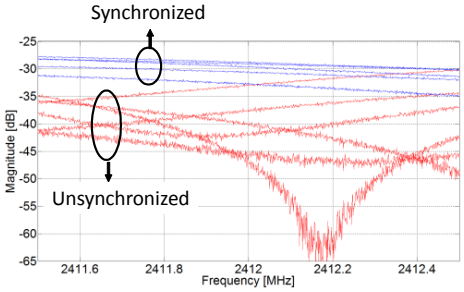

Fig. 5. Instantaneous channel magnitudes of unsynchronized (lower, red) and synchronized (upper, blue) cases. In this measurement setup, the small reverberation chamber was loaded with two absorbers with a horn transmit antenna and a patch receive antenna.

a-factor in Figs. 6 and 7, respectively. Curves for B_{re} are very similar and are not shown here. From these kernel fits, we see that there is a separation between the synchronized and unsynchronized cases. This indicates that the *a*-factor, B_{rc} and B_{re} have predictive value for the VST's performance. In the next section a logistic regression analysis is performed to quantitatively determine and compare the predictive value of these three metrics.

Figs. 6 and 7 show that neither the correlation metrics nor the *a*-factor by itself accurately predict the synchronization of the VST for every channel. There is some overlap in the curves, where, for the same value of B_{rc} or a-factor, the receiver does not synchronize. This is expected from Fig. 2, where we see that the size of the *a*-factor with respect to the coherence bandwidth also plays a role in determining whether a channel is correlated sufficiently for successful synchronization and demodulation.

IV. Analysis

To quantify the ability of these metrics to predict receiver synchronization, we used a logistic regression analysis. Logistic regression analysis is used, because the outcome is dichotomous and the predictive values of the different metrics are normalized, making comparison between the different metrics possible. The logistic function given by [17] was used as a model:

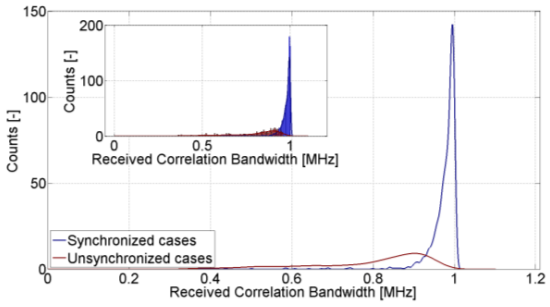

Fig. 6. Histogram of the received correlation bandwidth B_{rc} calculated from (5) with the complex data. Unsynchronized (red, lower count) and synchronized (blue, higher count) cases overlap somewhat. The large reverberation chamber was loaded with two stacks of three absorbers ("6 Abs Patch" in Table I), and the transmit and receive antennas were a horn and a patch, respectively.

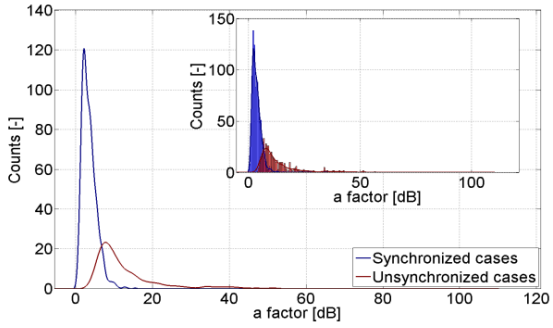

Fig. 7. Histogram of *a*-factor divided into unsynchronized (red) and synchronized (blue) cases. The chamber loading, antenna used, and data collection was identical to the results in Fig. 6.

$$p(X) = \frac{e^{\beta_0+\beta_1 X_1+\cdots+\beta_p X_p}}{1+e^{\beta_0+\beta_1 X_1+\cdots+\beta_p X_p}}\ , \tag{7}$$

where $p(X)$ is the probability that X occurs, β_0, ... , β_p are p regression coefficients, $X = (X_1, \ldots, X_p)$ are p predictors.

The regression coefficients were estimated for the different measurement setup configurations by use of a maximum likelihood method. The prediction was then made by equating the probability against a probability threshold for the same data set. If the calculated probability exceeded the probability threshold, it was deemed to have predicted system synchronization. The predictive values for the different measurement set-up configurations and metrics were then determined by the following equation

$$P_V = \left(w_s \frac{P_{Ns}}{M_{Ns}} + w_u \frac{P_{Nu}}{M_{Nu}}\right)/(w_s + w_u)\ , \tag{8}$$

where P_V is the predictive value with values between 0 and 1, P_{Ns} is the number of correctly predicted synchronized cases, P_{Nu} is the number of correctly predicted unsynchronized cases, M_{Ns} is the total number of measured synchronized cases, M_{Nu} is the total number of measured unsynchronized cases, and w_s and w_u are the weights for the synchronized and unsynchronized cases, respectively. We chose the weights for the synchronized and unsynchronized cases to be equal. This measure, also known as balanced accuracy, is used in binary classification settings to avoid biasing the accuracy towards the more frequent outcome [18]. Preliminary processing showed that the predictive value was highest when the probability threshold was chosen to be 0.7. The predictive values for different measurement setup configurations and the different metrics for the logistic regression analysis are shown in Table II.

Using the channel data obtained with the VNA, we achieved high predictive values up to 0.97 in the case of a heavily-loaded, small reverberation chamber. The predictive value of the unloaded large chamber was around 0.5 for all different antennas, which indicates that we cannot predict whether or not the test system will synchronize. The predictive

TABLE II. Predictive values of the logistic regression model

Measurement setup		Metrics used for logistic regression analysis			
		B_{rc}	B_{re}	a	(B_{rc} + B_{re} + a) **
Small Reverberation Chamber	0 Abs Helix	0.85	0.87	0.73	0.88
	0 Abs Horn	0.86	0.87	0.78	0.89
	0 Abs Patch	0.86	0.88	0.76	0.88
	1 Abs Helix	0.93	0.94	0.92	0.92
	1 Abs Horn	0.95	0.95	0.90	0.94
	1 Abs Patch	0.94	0.94	0.93	0.94
	2 Abs Helix	0.90	0.90	0.97	0.96
	2 Abs Horn	0.97	0.997	0.96	0.97
	2 Abs Patch	0.92	0.92	0.95	0.97
Large Reverberation Chamber	0 Abs Helix	0.55	0.50	0.50	0.60
	0 Abs Horn	0.50	0.50	0.50	0.55
	0 Abs Patch	0.50	0.50	0.50	0.50
	3 Abs Helix	0.87	0.86	0.83	0.88
	3 Abs Horn	0.86	0.85	0.76	0.86
	3 Abs Patch	0.90	0.90	0.81	0.90
	6 Abs Helix	0.86	0.87	0.84	0.87
	6 Abs Horn	0.91	0.992	0.89	0.93
	6 Abs Patch	0.91	0.92	0.89	0.91
Average*		0.836	0.842	0.801	0.853

*The average was taken over all cases including the unloaded cases
**The predictive value is calculated using all metrics

values in Table II of B_{rc} and B_{re} vary by less than 0.02 from each other. This indicates that we can characterize an instantaneous channel in a reverberation chamber sufficiently using a spectrum analyzer to measure the magnitude of the channel. Comparing the *a*-factor to B_{rc} and B_{re}, we see that B_{rc} and B_{re} are better at predicting whether the test system is able to synchronize. This is as expected, since the *a*-factor only considers the peak-to-minimum frequency information in the signal bandwidth. For example, the *a*-factor gives the same value for a frequency-selective deep fade for wideband and narrowband signals, while the effect on the wideband signal can be smaller when the information is distributed over all frequencies. However, we still see a reasonably high predictive value of 0.8 when using the *a*-factor for this system, and this metric is very efficient to compute.

V. UNCERTAINTY

We can estimate the measurement uncertainty by considering the reproducibility of both the VNA and VST measurements. The channel response and the EVM were measured at six different paddle positions, repeated ten times. For the VNA, the relative standard deviation at each frequency was calculated by dividing the standard deviation by the mean. The result was averaged over frequency in the signal bandwidth. The calibrated VNA's measurement uncertainty is 0.1 dB according to the instrument specifications, which is equivalent to 1.2%. The combined uncertainty for the VNA measurement was determined by taking the root sum of the square of the uncertainties. The worst-case scenario results in an error of 3.1% for the channel response measurements. For the VST, we again determined the relative standard deviation. The VST's sensitivity for the EVM measurement is lower than 1% according to the instrument specifications; taking this into account results in a total uncertainty of 1.3% for EVM measurements.

VI. CONCLUSION

We investigated how well different metrics could predict the performance of a wireless digital communication test system in a reverberation chamber. Testing was performed in two different reverberation chambers with several loading cases and several antennas. Using the logistic regression analysis, we showed that the reverberation chamber's instantaneous channel behavior, described by the *a*-factor, B_{rc} and B_{re} could predict whether or not the test system would be able to synchronize. The predictive values of the metrics improved considerably once loading was added to the chambers.

We have shown that the *a*-factor has a predictive value that is comparable to the predictive values of B_{rc} and B_{re}. Furthermore, the instantaneous channel of a reverberation chamber can be sufficiently characterized by the received correlation bandwidth with only the magnitude of the channel to predict the performance of the test system. The work here indicates that a relatively simple metric, the *a*-factor, which is the peak-to-minimum in the signal bandwidth, is a reasonable predictor of a digital wireless communication test system's performance, requiring no time-consuming autocorrelation function evaluation.

ACKNOWLEDGMENT

The authors thank Dr. Christopher L. Holloway of the NIST Boulder Laboratories and Prof. Frank Leferink of the University of Twente for their support.

REFERENCES

[1] D. A. Hill, Electromagnetic Fields in Cavities, New York: IEEE Press, 2009.

[2] "Electromagnetic Immunity - Off-Vehicle Source (Reverberation Chamber Method) - Part 16 - Immunity to Radiated Electromagnetic Fields," SAE J551/16, 2012.

[3] C. Orlenius, P.-S. Kildal and G. Poilasne, "Measurements of total isotropic sensitivity and average fading sensitivity of CDMA phones in reverberation chamber," in IEEE Antennas and Propagation Society International Symposium, Washington, D.C., 2005.

[4] V. Monebhurrun and T. Letertre, "Total radiated power measurements of WiFi devices using a compact reverberation chamber," in 20th International Zürich Symposium on Electromagnetic Compatibility, Zürich, 2009.

[5] J. H. Rudander, Ikram-e-Khuda, P.-S. Kildal and C. Orlenius, "Measurements of RFID Tag Sensitivity in Reverberation Chamber," IEEE Antennas and Wireless Propagation Letters, vol. 10, pp. 1345-1348, 2011.

[6] O. Delangre, P. De Doncker, F. Horlin, M. Lienard and P. Degauque, "Reverberation chamber environment for testing communication systems: applications to OFDM and SC-FDE," in IEEE 68th Vehicular Technology Conference, Calgary, 2008.

[7] P.-S. Kildal, C. Orlenius and J. Carlsson, "OTA testing in multipath of antennas and wireless devices with MIMO and OFDM," Proceedings of the IEEE, vol. 100, no. 7, pp. 2145-2157, 2012.

[8] S. J. Floris, K. A. Remley and C. L. Holloway, "Bit error rate measurements in reverberation chambers using real-time vector receivers," IEEE Antennas and Wireless Propagation Letters, vol. 9, pp. 619-622, 2010.

[9] K. A. Remley, S. J. Floris, H. A. Shah and C. L. Holloway, "Static and dynamic propagation-channel impairments in reverberation chambers," IEEE Transactions on Electromagnetic Compatibility, vol. 53, no. 3, pp. 589-599, 2011.

[10] C. L. Holloway, D. A. Hill, J. M. Ladbury, P. F. Wilson, G. Koepke and J. Coder, "On the use of reverberation chambers to simulate a Rician radio environment for the testing of wireless devices," IEEE Transactions on Antennas and Propagation, vol. 54, no. 11, pp. 3167-3177, 2006.

[11] X. Chen, P.-S. Kildal and S.-H. Lai, "Estimation of average Rician K-factor and average mode bandwidth in loaded reverberation chamber," Antennas and Wireless Propagation Letters, IEEE, vol. 10, pp. 1437-1440, 2011.

[12] X. Chen and P.-S. Kildal, "Theoretical derivation and measurements of the relationship between coherence bandwidth and RMS delay spread in reverberation chamber," EuCAP 2009, pp. 2687-2690, 2009.

[13] W. C. Jakes, Microwave Mobile Communications, Wiley-IEEE Press, 1994, pp. 45-61.

[14] W. T. C Burger, K. A. Remley, C. L. Holloway and J. M. Ladbury, "Proximity and antenna orientation effects for large-form-factor devices in a reverberation chamber," in 2013 IEEE International Symposium on Electromagnetic Compatibility (EMC), 2013.

[15] M. D. McKinley, K. A. Remley, M. Myslinski, J. S. Kenney, D. Schreurs and B. Nauwelaers, "EVM calculation for broadband modulated signals," in *64th ARFTG Conf. Dig*, 2004.

[16] M. I. Andries, P. Besnier and C. Lemoine, "On the prediction of the average absorbing cross section of materials from coherence bandwidth measurements in reverberation chamber," in International Symposium on Electromagnetic Compatibility, Rome, 2012.

[17] G. James, D. Witten, T. Hastie and R. Tibshirani, An Introduction to Statistical Learning with Applications in R, New York: Springer, 2014.

[18] K.H. Brodersen, C.S. Ong, K.E. Stephan and J.M. Buhmann, "The Balanced Accuracy and Its Posterior Distribution," in 20th International Conference on Pattern Recognition (ICPR), pp. 3121-3124, Aug. 2010.